

NASA/TM—2002-211210



Creep Behavior of Near-Stoichiometric Polycrystalline Binary NiAl

S.V. Raj
Glenn Research Center, Cleveland, Ohio

January 2002

The NASA STI Program Office . . . in Profile

Since its founding, NASA has been dedicated to the advancement of aeronautics and space science. The NASA Scientific and Technical Information (STI) Program Office plays a key part in helping NASA maintain this important role.

The NASA STI Program Office is operated by Langley Research Center, the Lead Center for NASA's scientific and technical information. The NASA STI Program Office provides access to the NASA STI Database, the largest collection of aeronautical and space science STI in the world. The Program Office is also NASA's institutional mechanism for disseminating the results of its research and development activities. These results are published by NASA in the NASA STI Report Series, which includes the following report types:

- **TECHNICAL PUBLICATION.** Reports of completed research or a major significant phase of research that present the results of NASA programs and include extensive data or theoretical analysis. Includes compilations of significant scientific and technical data and information deemed to be of continuing reference value. NASA's counterpart of peer-reviewed formal professional papers but has less stringent limitations on manuscript length and extent of graphic presentations.
- **TECHNICAL MEMORANDUM.** Scientific and technical findings that are preliminary or of specialized interest, e.g., quick release reports, working papers, and bibliographies that contain minimal annotation. Does not contain extensive analysis.
- **CONTRACTOR REPORT.** Scientific and technical findings by NASA-sponsored contractors and grantees.

- **CONFERENCE PUBLICATION.** Collected papers from scientific and technical conferences, symposia, seminars, or other meetings sponsored or cosponsored by NASA.
- **SPECIAL PUBLICATION.** Scientific, technical, or historical information from NASA programs, projects, and missions, often concerned with subjects having substantial public interest.
- **TECHNICAL TRANSLATION.** English-language translations of foreign scientific and technical material pertinent to NASA's mission.

Specialized services that complement the STI Program Office's diverse offerings include creating custom thesauri, building customized data bases, organizing and publishing research results . . . even providing videos.

For more information about the NASA STI Program Office, see the following:

- Access the NASA STI Program Home Page at <http://www.sti.nasa.gov>
- E-mail your question via the Internet to help@sti.nasa.gov
- Fax your question to the NASA Access Help Desk at 301-621-0134
- Telephone the NASA Access Help Desk at 301-621-0390
- Write to:
NASA Access Help Desk
NASA Center for AeroSpace Information
7121 Standard Drive
Hanover, MD 21076

NASA/TM—2002-211210



Creep Behavior of Near-Stoichiometric Polycrystalline Binary NiAl

S.V. Raj
Glenn Research Center, Cleveland, Ohio

Prepared for the
131st Annual Meeting and Exhibition
sponsored by The Minerals, Metals, and Materials Society
Seattle, Washington, February 17–21, 2002

National Aeronautics and
Space Administration

Glenn Research Center

Available from

NASA Center for Aerospace Information
7121 Standard Drive
Hanover, MD 21076

National Technical Information Service
5285 Port Royal Road
Springfield, VA 22100

Available electronically at <http://gltrs.grc.nasa.gov/GLTRS>

CREEP BEHAVIOR OF NEAR-STOICHIOMETRIC POLYCRYSTALLINE BINARY NiAl

S.V. Raj
National Aeronautics and Space Administration
Glenn Research Center
Cleveland, Ohio 44135

SUMMARY

New and published constant load creep and constant engineering strain rate data on near-stoichiometric binary NiAl in the intermediate temperature range 700 to 1300 K are reviewed. Both normal and inverse primary creep curves are observed depending on stress and temperature. Other characteristics relating to creep of NiAl involving grain size, stress and temperature dependence are critically examined and discussed. At stresses below 25 MPa and temperatures above 1000 K, a new grain boundary sliding mechanism was observed with $n \sim 2$, $Q_c \sim 100 \text{ kJ mol}^{-1}$ and a grain size exponent of about 2. It is demonstrated that Coble creep and accommodated grain boundary sliding models fail to predict the experimental creep rates by several orders of magnitude.

INTRODUCTION

Over the last several decades, a considerable amount of research has been conducted on developing NiAl-based alloys for use as airfoils in gas-turbine aircraft engines. More recently, NiAl is being examined as an environmentally protective top coating on turbine blades in aircraft engines and combustor liners in advanced space reusable launch vehicles. An attractive combination of oxidation, physical and thermal properties makes NiAl a desirable material for these applications. However, the inherent low temperature brittleness of the material combined with its poor elevated temperature creep properties have prevented an exploitation of these characteristics for many of these structural applications.

A fundamental understanding of the creep mechanisms dominant in NiAl is important to improve its high temperature creep properties. As a result, several investigators have conducted constant engineering strain rate (refs. 1 to 4) and constant stress or constant load creep (refs. 5 to 17) tests on polycrystalline binary NiAl at elevated temperatures in order to characterize and elucidate the governing mechanisms dominating creep behavior. Despite this, there are inconsistencies in the reported observations and a lack of a clear understanding of the fundamental mechanisms controlling creep in this alloy. The first detailed investigation of the elevated temperature compressive properties of near-stoichiometric and nonstoichiometric NiAl was conducted by Mukherjee and his colleagues in the mid-1960's (ref. 1), who reported that a viscous creep mechanism was dominant at very high temperatures while a process with a stress dependent activation energy was dominant at intermediate temperatures. Although they observed values of the power-law creep stress exponent, $n \approx 3.5$ between 1523 and 1748 K in near-stoichiometric polycrystalline NiAl, later observations have revealed that $n > 4$ for this alloy at lower temperatures typically between 1000 and 1400 K (table I). For example, coarse-grained near-stoichiometric NiAl, with grain sizes, $d > 450 \mu\text{m}$, typically exhibits $n \approx 4.0$ to 4.5, whereas values of $n \approx 5.5$ to 7.5 appear to be typical for fine-grained NiAl with $d < 40 \mu\text{m}$ at intermediate stresses (ref. 15). Curiously, the reported values of the activation energy for creep, Q_c , for polycrystalline NiAl are generally about 300 kJ mol^{-1} (refs. 1 to 3, 7, and 13 to 16) in the power-law creep regime irrespective of the magnitude of n . However, higher values of Q_c much greater than 300 kJ mol^{-1} have also been reported (refs. 17 to 19).

An examination of the published creep data on near-stoichiometric binary NiAl reveals several points. First, a vast majority of the data have been obtained under compression loading conditions, and long term tensile creep data are virtually nonexistent in the literature. This sparsity in tensile creep data raises the question as to whether compression and tensile creep data are comparable. Second, there is little information correlating the dislocation substructures that form in this alloy with its creep behavior. Third, the effect of grain size on the power-law creep behavior of NiAl is contrary to observations in pure metals (ref. 4). Fourth, there is a discrepancy in the characteristics of the creep mechanism occurring at low stresses (refs. 11, 13, and 16).

The objectives of this paper are to review the current state of knowledge on the creep of near-stoichiometric polycrystalline NiAl with a view of addressing the above issues. Specifically, compression and tensile creep data obtained on similarly processed material are compared. The creep behavior and the corresponding dislocation substructure of cast and extruded NiAl are compared with the observed results on powder metallurgy (PM)-extruded NiAl. Next, grain size effects in the power-law creep region are examined. Finally, the characteristics of the low stress creep mechanism are discussed.

CREEP BEHAVIOR AT INTERMEDIATE STRESSES

The Shape Of The Creep Curves

Figure 1(a) shows the tensile constant load creep curves, plotted as the true creep rate, $\dot{\epsilon}$, against true strain, ϵ , for cast and extruded NiAl between 700 and 1200 K under initial stresses varying from 25 to 150 MPa. Similar $\dot{\epsilon} - \epsilon$ plots are shown in figure 1(b) for PM-extruded NiAl (PM-1) with $d \approx 23 \mu\text{m}$ tested under a constant compressive load between 1000 and 1300 K under initial stresses varying from 25 to 51 MPa (ref. 13). Unlike pure metals, where steady-state creep behavior may occur typically when $\epsilon > 10$ percent, NiAl often exhibits quasi-steady-state behavior when $\epsilon > 2$ percent. The effect of a change in the cross-sectional area during deformation is evident beyond the primary creep region, where $\dot{\epsilon}$ generally increases for the tensile (fig. 1(a)) and decreases (fig. 1(b)) for the compressive curves, respectively, with increasing ϵ .

Figures 1(a) and (b) show broad similarities in their primary creep behavior. The creep rate decreases sharply soon after loading followed by a primary creep transient which exhibits two distinct shapes: Normal primary creep is observed at high stresses and temperatures and inverse primary creep occurs at low stresses and temperatures. Inverse primary creep behavior, which has been observed in solid solution alloys (ref. 20), LiF (ref. 21) and NiAl polycrystals (ref. 7), is generally attributed either to the inhibition of dislocation nucleation or to low dislocation mobility in the material during deformation. In the case of NiAl, the initial extruded microstructure was fully recrystallized with few observable dislocations (ref. 22). Despite this observation, two factors rule out the possibility that dislocation nucleation is inhibiting creep under the stress and temperature conditions reported in this study. First, noting that dislocation nucleation is an athermal process, the transition from inverse to normal primary creep with increasing temperature seen in figures 1(a) and (b) indicates that creep in this alloy is primarily restricted by dislocation mobility rather than dislocation nucleation. Second, the creep behavior of the alloy at 700 K changes from inverse to normal primary creep with increasing stress with a corresponding estimated increase in the dislocation density of about a factor of 1.5 (fig. 1(a)). Therefore, it must be concluded that inverse primary creep is due to low dislocation mobility. A similar conclusion was reached by Forbes, et al. (ref. 23), who observed that the creep of NiAl single crystals oriented in the "hard" $\langle 001 \rangle$ and the "soft" $\langle 223 \rangle$, $\langle 111 \rangle$ and $\langle 110 \rangle$ orientations were dislocation mobility-controlled, although in the case of the "hard" crystals, they suggested a dislocation substructure-controlled process was also important.

Stress Dependence Of The Secondary Creep Rate

Double logarithmic plots of the true secondary creep rate against true stress are shown in figures 2(a) and (b) for the coarser-grained ($d \approx 35$ to $39 \mu\text{m}$) cast-extruded NiAl tested under compression and tensile loading, respectively, between 700 and 1200 K (ref. 15). The $\dot{\epsilon} - \sigma$ data shown in figure 2(c) for the finer-grained ($d \approx 23 \mu\text{m}$) PM-extruded material (PM-1) were determined in compression creep between 1000 and 1300 K (refs. 11 and 13). The straight lines in the figures indicate the positions of the linear regression fits to the data. The data from literature sources on materials with similar values of grain size are also included in figure 2(c) for comparison (refs. 3 and 22). Assuming a power-law creep relation, the stress exponent, n , varies between 4.9 (at 1000 K) and 8.7 (at 800 K) at intermediate compressive stresses for the cast-extruded NiAl compressed between 800 and 1200 K (fig. 2(a)). There is a significant deviation from linearity above 170 MPa at 800 K. The tension creep results show that n is about 5.5 and 5.8 at 1100 and 1200 K, respectively, but varies between 9.7 and 15.0 below 1100 K (fig. 2(b)). The PM-extruded specimens exhibit similar values of n varying between 5.8 and 7.4 at intermediate stresses (fig. 2(c)). In addition, the finer-grained powder-metallurgy material also exhibits a different creep regime with a stress exponent of about 2 (fig. 2(c)).

Details of the values of n and Q_c observed at intermediate stresses corresponding to the intermediate stress region are tabulated in table I for the data shown in figures 2(a) to (c) as well as those reported in the literature for near-stoichiometric polycrystalline NiAl (refs. 1 to 3, 7, 9, 10, 14, and 16). An examination of the reported values of the power-law creep stress exponent for NiAl at intermediate stresses in a similar range of stresses and temperatures reveals that the data appear to fall into two broad categories: (a) fine-grained NiAl with $d < 40 \mu\text{m}$ typically exhibits values of $n \approx 5.0$ to 7.5 ; (b) coarse-grained NiAl with $d > 150 \mu\text{m}$ often exhibits $n \approx 3.5$ to 4.5 (refs. 2, 15 and 16) (table I). More recently, Artz and Grahle, (ref. 16) have reported values of $n \approx 4.5$ and 7.3 for coarse ($d \approx 170 \mu\text{m}$) and fine-grained ($d \approx 20 \mu\text{m}$) NiAl, respectively, under similar stress and temperature conditions. The absolute difference in the values of n for the fine and coarse-grained NiAl varies between 2 and 3. This observation is especially interesting in view of the fact that the stress exponents, n' , measured from stress decrease tests in “constant substructure” experiments often reveal that $n' = n + \delta$, where δ varies between 2 and 3 (ref. 24). Thus, the creep rate can be expressed as a function of the applied stress as

$$\dot{\epsilon} = A \left(\frac{b}{d} \right)^p \left(\frac{D_0 G b}{kT} \right) \left(\frac{\sigma}{G} \right)^{n+\delta} \left(\frac{\lambda_s}{b} \right)^\delta \exp \left(-\frac{Q_c}{RT} \right) \quad (1)$$

where b is the Burgers vector, D_0 is the frequency factor, G is the shear modulus, k is Boltzmann’s constant, λ_s is the equivalent subgrain size, R is the universal gas constant, T is the absolute temperature, and A' and p are dimensionless constants. The equilibrium subgrain size, d_s , is inversely dependent on the applied stress through the relation (ref. 25)

$$\frac{d_s}{b} = 23 \left(\frac{G}{\sigma} \right) \quad (2)$$

Whittenberger (ref. 2), and Artz and Grahle (refs. 14 and 16) have reasoned that coarse-grained NiAl with $d > d_s$ is likely to develop well-formed subgrains during creep so that $\lambda_s \approx d_s$ in equation (1). Thus, combining equations (1) and (2) results in a stress dependence described by n , where the experimental observations indicate that $n \approx 3.5$ to 4.5 (refs. 1, 7, 10, and 16). Correspondingly, the creep of fine-grained NiAl with $d \leq d_s$ was assumed to be equivalent to conducting a “constant substructure” test, where now $\lambda_s \approx d$ in equation (1), and the observed stress exponents are $n' = n + \delta \approx 5.0$ to 7.5 (refs. 2, 3, 11, 13 to 16, and 22).

Although at first glance this explanation appears to rationalize the observed values of n for the coarse and fine-grained NiAl in an elegant and simple manner, on closer scrutiny certain inconsistencies become apparent. First, the values of n reported in the literature decrease steadily with increasing temperature with n approaching 3 above 1500 K (refs. 1, 18, and 23). This trend is clearly evident in both the coarse-grained data of Vandervoort, et al. (ref. 1) and Yang and Dodd (ref. 7) as well as the single crystal data of Forbes, et al. (ref. 23). In fact, a comparison of the stress exponents reported for several polycrystalline data under similar stress and temperature conditions reveals that they are essentially independent of grain size (ref. 17). Nevertheless, it is intriguing that Artz and Grahle, (refs. 14 and 16) have reported two different values of n under similar stress and temperature conditions (table I), although it is unclear if grain growth during creep was significant in their tests. Second, substituting d for d_s in equation (2), the critical stress, σ_c , above which the equilibrium subgrain size should be less than the grain size, can be estimated. For $d \sim 35 \mu\text{m}$, the estimated magnitudes of σ_c for the cast extruded NiAl data shown in figures 2(a) and (b) are 12 to 15 MPa in the temperature range 800 to 1200 K. Similarly, with $d_s \sim 23 \mu\text{m}$ for the PM-extruded alloy shown in figure 2(c), σ_c varies between 18 and 21 MPa. Since most of the data shown in figures 2(a) to (c) were determined at stresses above σ_c so that $d_s < d$, the “constant substructure” hypothesis would predict that $n \sim 3.5$ to 4.5 . Clearly, this is not the case with the data shown in figures 2(a) to (c) since the observed values of n are typically much greater than 5 with $n \gg 6$ below 1000 K . This is true even if allowance is made for the fact that these estimated values of σ_c could vary by a factor of 2. Similar calculations for the data reported by Artz and Grahle (refs. 14 and 16) reveals that σ_c varies between 19 and 21 MPa for the fine-grained material. Once again, most of their data were determined under stresses higher than σ_c , where reported value of n was 7 rather than about 4.5 as observed in their coarse-grained alloy. Third, the “constant substructure” model assumes that well-formed subgrains will develop during creep, and implicitly predicts normal primary creep transient curves. As shown in figures 1(a) and (b), inverse primary creep transients are often observed at low temperatures and stresses even when $\sigma > \sigma_c$. Since observations in many solid solution alloys suggest that inverse primary transients are generally associated with

a homogenous dislocation substructure (ref. 20), it is once again doubtful whether the “constant substructure” model adequately explains the experimental results. Fourth, the deformation substructures are not always consistent with the expectations of the “constant substructure” hypothesis. For example, Whittenberger (ref. 2) observed well developed subgrains above σ_c in fine-grained PM-extruded NiAl. In contrast, Raj and Farmer (refs. 11 and 13) reported that the substructure formed in crept PM-extruded NiAl with a similar grain size consisted of a mixture of subgrains, sub-boundaries, cells, dislocation tangles, dipoles and loops at stresses exceeding σ_c , where the microstructure often varied with grain size within the same transmission electron microscopy (TEM) foil (fig. 3). Curiously, small grains appeared to possess smaller subgrains and a higher density of dislocations than the larger grains. A similar observation of dislocation loops, dipoles, jogged dislocations and dislocation tangles have been reported in NiAl single crystals (ref. 5) as well as polycrystals (ref. 7) from which it was concluded that dislocation cross-slip was the rate controlling creep mechanism. Similarly, Raj et al. (refs. 15 and 26) reported that while well-formed subgrains were observed in some grains of the cast and extruded crept specimens (fig. 4(a)), most grains were virtually devoid of any substantial dislocation substructure at 1100 and 1200 K under stresses exceeding σ_c even after $\epsilon > 10$ percent with only isolated dislocations and rudimentary dislocation networks observed in some grains (fig. 4(b)). The observed microstructural differences in the crept PM-extruded and cast and extruded NiAl appear to be due to the presence of alumina particles in the PM material. In contrast to the cast and extruded NiAl, where dislocations generated at a grain boundary can zip across the grain to the opposite boundary, the alumina particles in the PM-extruded material are likely to anchor the mobile dislocations thereby resulting in the formation of dislocation substructures.

Alternatively, it has been suggested that values of $n > 3$ stem from the contributions of nondiffusional dislocation mechanisms, such as cross-slip, lattice-controlled and obstacle-controlled glide, to creep (ref. 27). Since the dominance of these dislocation processes are likely to increase with increasing stress and decreasing temperatures, the tendency to deviate from true steady-state creep behavior correspondingly increases. Thus, n is expected to decrease towards a value of 3 with decreasing stresses and increasing temperature in conformity with experimental observations (refs. 1, 18, and 23).

Activation Energy For Creep

Figure 5 compares the stress dependence of Q_c determined from the data shown in figures 2(a) to (c). The broken horizontal lines represent the measured values of the activation energy for lattice self-diffusion, $(Q_l)_{Ni}$ (ref. 28). The experimental value of grain boundary diffusion, $(Q_{gb})_{Ni} \approx 335 \text{ kJ mol}^{-1}$ (ref. 29) is not indicated in the figure for clarity. The activation energy data shown in figure 5 clearly correspond to three distinct deformation regimes with the approximate transition stresses being about 25 and 70 MPa in traversing from regions I to II and from II to III, respectively. The activation energy for creep is much less than $(Q_l)_{Ni}$ in region I, where it is about 95 kJ mol^{-1} (refs. 11 and 13). In regime II, Q_c is independent of stress whereas it exhibits an inverse linear dependency on the applied stress in region III. Other investigators have also observed similar stress dependencies in Q_c (refs. 1 and 7) (table I), where estimates of the apparent activation volume for creep were found to be 75 to 100 b^3 (refs. 1 and 13). It has been demonstrated elsewhere that region III corresponds to the exponential creep regime (ref. 13). The magnitudes of Q_c in region II determined from compression creep tests are about 300 kJ mol^{-1} for both cast and PM-extruded NiAl with the corresponding values of n lying between 4.9 and 6.2 (refs. 11, 13, and 15). This value is in reasonable agreement with that for lattice self-diffusion of Ni in NiAl (ref. 28) as well as other published values for the activation energy for creep for both coarse and fine-grained materials (table I). In contrast, the activation energy for creep determined from the tension creep experiments were closer to about 400 kJ mol^{-1} in Region II, which is substantially larger than those observed in the compression tests. Although values of Q_c ranging from about 355 to 440 kJ mol^{-1} have been reported for both single and polycrystalline NiAl in some investigations (refs. 17 and 18, and 23), no clear rationale has been advanced for their observance.

Grain Size Effects

As discussed earlier, the “constant substructure” rationale does not provide a consistent picture with the experimental observations. Therefore, the stress dependency of the secondary creep rate as reflected by the magnitude of n is not influenced directly by grain size. However, grain size does appear to influence the magnitude of the creep rate in FeAl and NiAl, where a grain size strengthening effect contradictory to observations in pure metals has been reported (ref. 4). This grain size strengthening effect is evident in figure 6, where the creep behaviors of

coarser-grained cast ($d \approx 35 \mu\text{m}$) and powder-metallurgy (PM-2 with $d \approx 39 \mu\text{m}$) extruded specimens are compared with that of a finer-grained PM-extruded specimen (PM-1 with $d \approx 23 \mu\text{m}$) at 1100 K under an initial stress of 40.0 MPa (ref. 15). It can be seen that the fine-grained material is significantly stronger than the coarser-grained specimens under these conditions. This result is contradictory to observations in other materials, where fine-grained specimens creep faster than the coarser-grained ones at similar values of grain size due to contributions from grain boundary sliding (ref. 2). A comparison of the dislocation substructure for the cast (fig. 4(b)) and PM-1 (fig. 3) suggests that the observed grain size strengthening may be due to the presence of a substantial dislocation substructure in the latter material during creep.

Creep Behavior At Low Stresses

Recently, Artz and Grahle (refs. 14 and 16) have reported that Coble creep with $n = 1$ and an estimated value of $Q_c \sim 143 \text{ kJ mol}^{-1}$ occurs in fine-grained ($d = 20 \mu\text{m}$) NiAl at low stresses. This estimated value of Q_c was attributed to the activation energy for grain boundary diffusion. While this transition to a low stress mechanism confirms the earlier observations of Raj and Farmer (refs. 11 and 13), the characteristics of the two processes, and hence, the conclusions on the nature of the rate-controlling mechanism are vastly different. As noted earlier, there is a transition to region I from region II with decreasing stress in the $Q_c - \sigma$ (fig. 5) plot, with a corresponding decrease in Q_c from 100 kJ mol^{-1} to $Q_c \approx 300 \text{ kJ mol}^{-1}$. This transition is also seen in figure 2(c), where $n \sim 2$ above 1100 K at the lower stresses for the fine-grained ($d \approx 23 \mu\text{m}$) PM-extruded NiAl (refs. 11 and 13). It should be noted that both values of Q_c reported in these two sets of investigations are much lower than the experimental value of $Q_{gb} \approx 335 \text{ kJ mol}^{-1}$ (ref. 29) (fig. 5). Since the experimentally measured value of $Q_{gb} > (Q_i)_{Ni}$, it is unclear if other factors such as grain boundary migration and grain boundary segregation had influenced these measurements (ref. 29).

The mechanism in regime I exhibits a normal primary creep transient behavior lasting for about 200 h (fig. 7(a)) and a grain size exponent of about 2 (fig. 7(b)). Clearly, if Coble creep was the dominant process in this regime, $p \sim 3$ in equation (1) and the primary creep transient behavior would be linear or at least exhibit a short normal characteristic lasting less than 10 h. Instead, figure 7(a) suggests that the process operating in region I is a dislocation-controlled mechanism. Further support for this conclusion comes from the detailed microstructural observations made in region I (refs. 11 and 13). Although most of the grains did not exhibit a prominent dislocation substructure in this deformation regime, isolated bands of dislocation loops were seen in some grains (fig. 8(a)), where they appeared to have been emitted from the grain boundaries (figs. 8(b) and (c)). These observations, taken together with the observed values of $n \sim 2$, $Q_c \sim 100 \text{ kJ mol}^{-1}$ and $p \sim 2$, suggest that the emission of these dislocation loops is due to an accommodated grain boundary sliding mechanism. Figure 9 compares the experimental creep rates observed at 1200 K with those predicted by Coble creep (refs. 31 and 32) and accommodated grain boundary sliding models, such as the Ball and Hutchinson mechanism (refs. 33 and 34). It is clear that the discrepancy between the experimental and the predicted rates for both the Coble and the current models for accommodated grain boundary sliding is

over five orders of magnitude primarily because $A = A' \approx 1.9 \times 10^{-6}$ in equation (1) for $\left(\frac{\sigma}{G}\right)^{n+\delta} \left(\frac{\lambda_s}{b}\right)^\delta \approx \left(\frac{\sigma}{G}\right)^n$. In

comparison, models for accommodated grain boundary sliding in disordered materials predict values of A between 75 and 150 (ref. 33). The reason for this discrepancy may lie in the fact that the current models for accommodated grain boundary sliding were developed for disordered materials, where site occupancy restrictions are unimportant. However, site occupancy restriction is very important for long range ordered materials like NiAl, where the Al atom is less likely to reside in a Ni site.

SUMMARY AND CONCLUSIONS

Constant load creep and constant engineering strain rate data on near-stoichiometric binary NiAl in the intermediate temperature range 700 to 1300 K are reviewed with the objective of characterizing and understanding the creep mechanisms dominant in this material. The primary creep curves showed two distinct forms depending on stress and temperature. First, at the lower temperatures and stresses, there was an initial sharp decrease in the creep rate soon after the application of the applied stress followed by inverse primary creep, where the creep rate increased monotonically towards a steady-state value. Second, at the higher temperatures and stresses, normal primary creep was observed after the specimen was loaded, where the creep rate decreased monotonically towards a steady-state value.

These observations suggest that primary creep in binary NiAl is limited by dislocation mobility. The effects of grain size on the creep stress exponent, n , and the validity of the “constant substructure” rationale for the observations are examined. It is shown that this explanation is inconsistent with other experimental observations. Instead, it is suggested that the observed variations in n are due to contributions from nondiffusional mechanisms, such as cross-slip, lattice-controlled and obstacle-controlled glide, whose importance increase with increasing stresses and decreasing temperatures. The activation energy for creep, Q_c , was constant in the power-law creep regime and equal to about 300 kJ mol^{-1} for the compression data. In contrast, $Q_c \approx 400 \text{ kJ mol}^{-1}$ for data obtained in the tension tests. The reason for this discrepancy between the two sets of results is unclear at present. Both the compression and tension data exhibit a stress dependent activation energy under conditions corresponding to exponential creep. At stresses below 25 MPa, a grain boundary sliding mechanism was observed with a stress exponent of about 2, an activation energy of about 100 kJ mol^{-1} and a grain size exponent of about 2. Bands of dislocation loops were observed to have been emitted from the grain boundaries during creep. It is demonstrated that Coble and accommodated grain boundary sliding models fail to predict the experimental creep rates by several orders of magnitude.

REFERENCES

1. R.R. Vandervoort, A.K. Mukherjee, and J.E. Dorn, *Trans. ASM*, **59** (1966), pp. 930–944.
2. J.D. Whittenberger, *J. Mater. Sci.*, **22** (1987), pp. 394–402.
3. J.D. Whittenberger, *J. Mater. Sci.*, **23** (1988), pp. 235–240.
4. J.D. Whittenberger, *Effect of Grain Size on the High Temperature Properties of B2 Aluminides*, NASA TM-101382 (Lewis Research Center, Cleveland, OH, 1987), pp. 1–24.
5. P.R. Strutt and R.A. Dodd, *Ordered Alloys—Structural Applications and Physical Metallurgy*, B.H. Kear, C.T. Sims, N.S. Stoloff, and J.H. Westbrook, eds. (Claitor’s Publishing Division, Baton Rouge, LA, 1970), pp. 475–504.
6. W.J. Yang, R.A. Dodd, and P.R. Strutt, *Metall. Trans.*, **3** (1972), pp. 2049–2054.
7. W.J. Yang and R.A. Dodd, *Met. Sci. J.*, **7** (1973), pp. 41–47.
8. A. Prakash and R.A. Dodd, *J. Mater. Sci.*, **16** (1981), pp. 2495–2500.
9. M. Rudy and G. Sauthoff, *High-Temperature Ordered Intermetallic Alloys*, vol. **39**, C.C. Koch, C.T. Liu, and N.S. Stoloff, eds. (Materials Research Society, Pittsburgh, PA, 1985), pp. 327–333.
10. M. Rudy and G. Sauthoff, *Mater. Sci. Eng.*, **81** (1986), pp. 525–530.
11. S.V. Raj and S.C. Farmer, *High-Temperature Ordered Intermetallic Alloys V*, vol. **288**, I. Baker, R. Darolia, J.D. Whittenberger, and M.H. Yoo, eds. (Materials Research Society, Pittsburgh, PA, 1993) pp. 647–652.
12. K. Sadananda, C.R. Feng, H.N. Jones, and J.J. Petrovic, *Structural Intermetallics (ISSI-1)*, R. Darolia, J.J. Lewandowski, C.T. Liu, P.L. Martin, D.B. Miracle, and M.V. Nathal, eds. (The Minerals, Metals and Materials Society, Warrendale, PA, 1993), pp. 809–818.
13. S.V. Raj and S.C. Farmer, *Metall. Mater. Trans. A*, **26A** (1995), pp. 343–356.
14. E. Artz and P. Grahle, *High-Temperature Ordered Intermetallic Alloys VI*, vol. **364**, J. Horton, I. Baker, S. Hanada, R.D. Noebe, and D.S. Schwartz, eds. (Materials Research Society, Pittsburgh, PA, 1995), pp. 525–536.
15. S.V. Raj, A. Garg, and T.R. Bieler, *High-Temperature Ordered Intermetallic Alloys VII*, vol. **460**, C.C. Koch, C.T. Liu, N.S. Stoloff, and A. Wanner, eds. (Materials Research Society, Pittsburgh, PA, 1997), pp. 473–478.
16. E. Artz and P. Grahle, *Acta Mater.*, **46** (1998), pp. 2717–2727.
17. T.A. Venkatesh and D.C. Dunand, *Metall. Mater. Trans. A*, **31A** (2000), pp. 781–792.
18. M.V. Nathal, *Ordered Intermetallics—Physical Metallurgy and Mechanical Behavior*, C.T. Liu, R.W. Cahn, and G. Sauthoff, eds. (Kluwer Academic Publishers, Dordrecht, The Netherlands, 1992), pp. 541–563.
19. J.D. Whittenberger, R.K. Viswanadham, S.K. Mannan, and B. Sprissler, *J. Mater. Sci.*, **25** (1990) pp. 35–44.
20. W.D. Nix and B. Ilschner, *Strength of Metals and Alloys*, vol. **3**, P. Hansen, V. Gerold and G. Kostorz, eds., (Pergamon Press, Oxford, 1980), pp. 1503–1530.
21. W.A. Coghlan, R.A. Menezes, and W.D. Nix, *Phil. Mag.*, **23** (1971), pp. 1515–1530.
22. R.R. Bowman, R.D. Noebe, S.V. Raj, and I.E. Locci, *Metall. Trans. A*, **23A** (1992), pp. 1493–1508.
23. K.R. Forbes, U. Glatzel, R. Darolia, and W.D. Nix, *Metall. Mater. Trans. A*, **27A** (1996), pp. 1229–1240.
24. O.D. Sherby, R.H. Klundt, and A.K. Miller, *Metall. Trans. A*, **8A** (1977), pp. 843–850.
25. S.V. Raj and G.M. Pharr, *Mater. Sci. Eng.*, **81** (1986), pp. 217–287.

26. S.V. Raj and A. Garg, unpublished research (Lewis Research Center, Cleveland, OH, 1995).
27. S.V. Raj and A.D. Freed, *Mater. Sci. Eng.*, **283A** (2000), pp. 196–202.
28. G.F. Hancock and B.R. McDonnell, *Phys. Stat. Sol. (a)*, **4** (1971), pp. 143–150.
29. J. Cermak, I. Stloukal, J. Ruzickova, and A. Pokorna, *Intermetall.* **6** (1998), pp. 21–28.
30. C.R. Barrett, J.L. Lytton, and O.D. Sherby, *Trans. AIME*, **239** (1967), pp. 170–180.
31. R.L. Coble, *J. Appl. Phys.*, **33** (1963), pp. 1671–1673.
32. W.R. Cannon and T.G. Langdon, *J. Mater. Sci.*, **23** (1988), pp. 1–20.
33. R.C. Gifkins and T.G. Langdon, *Mater. Sci. Eng.*, **36** (1978), pp. 27–33.
34. A. Ball and M.M. Hutchinson, *Met. Sci. J.*, **3** (1969), pp. 1–7.

TABLE I.—VALUES OF THE STRESS EXPONENT AND THE CREEP ACTIVATION ENERGY OBSERVED IN NEAR-STOICHIOMETRIC POLYCRYSTALLINE NiAl AT INTERMEDIATE STRESSES IN THE POWER-LAW CREEP REGIME

Al, at.%	Processing	Testing mode ^a	d, μm	T, K	n	Q_c , kJ mol^{-1}	Reference
49.6	Cast	CSR; C	1130	1073 to 1748	3.3 to 6.9	290; stress dependent Q_c when $\sigma > 13.8$ MPa	1
50.0	Cast and annealed at 1573 K/?	CL; C	450	1073 to 1318	4.6 to 10.2	285; stress and temperature dependent Q_c when $\sigma > 55.2$ MPa and $T < 1223$ K	7
50.0	Cast and annealed at 1473 K/24 h	CL; C	500 to 600	1173	4.7	-----	9 and 10
49.8 to 50.6	Cast and extruded	CL; T	39	700 to 1200	5.5 to 15.0	400; stress dependent Q_c when $\sigma > 40$ MPa	Present study
50.3	Cast and extruded	CL; C	35	800 to 1200	4.9 to 8.7	300; Q_c when $\sigma > 75$ MPa	15
49.2 to 50.6	PM-extruded	CSR; C	13 to 17	1200 to 1400	5.5 to 6.5	305 to 310	2
50.6	PM-extruded	CL; C	23	1000 to 1300	5.8 to 7.4	290 to 300; stress dependent Q_c when $\sigma > 55$ MPa	11 and 13
50.4	PM-extruded; PM-extruded and annealed at 1723 K/50h	CL; C	20; 170	1300 to 1473; 1300 to 1400	7.3; 4.5	290; 300	14 and 16
NiAl ^b	Reactive infiltration	CL; C	200	988 and 1298	5.5 and 5.6	375	17

^aC = compression; CL = constant load; CSR = constant strain rate; T = tension.

^bThe exact composition of the tested specimens was not reported. The reactive infiltrated ingot showed a linear variation in the Al content from about 36 to 47 (at.%) for a linear traverse of about 27 mm along the ingot.

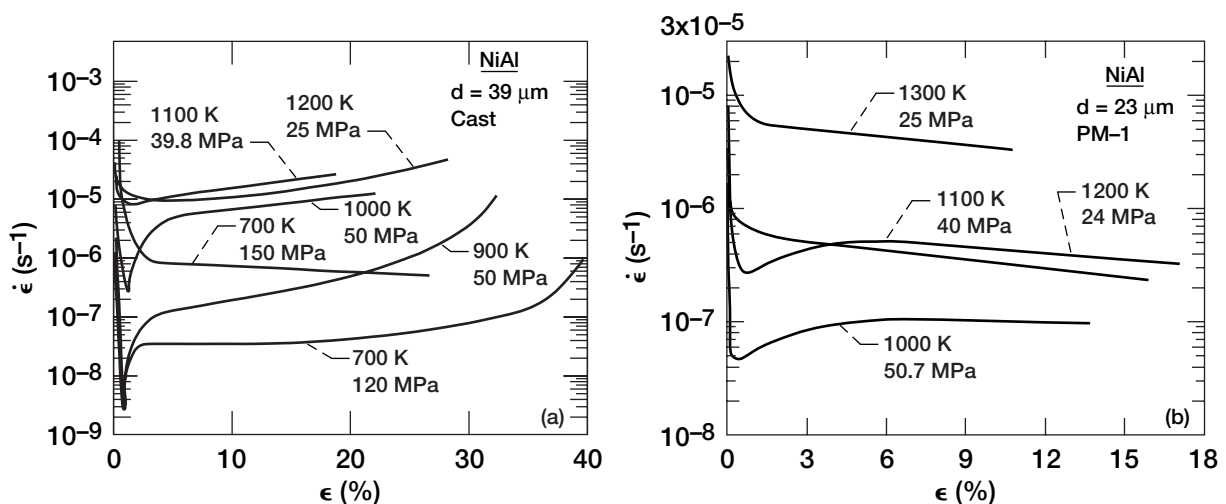


Figure 1.—True creep rate versus true strain plots for (a) cast and extruded, and (b) PM-extruded (ref. 13) polycrystalline near-stoichiometric NiAl tested in tension and compression, respectively.

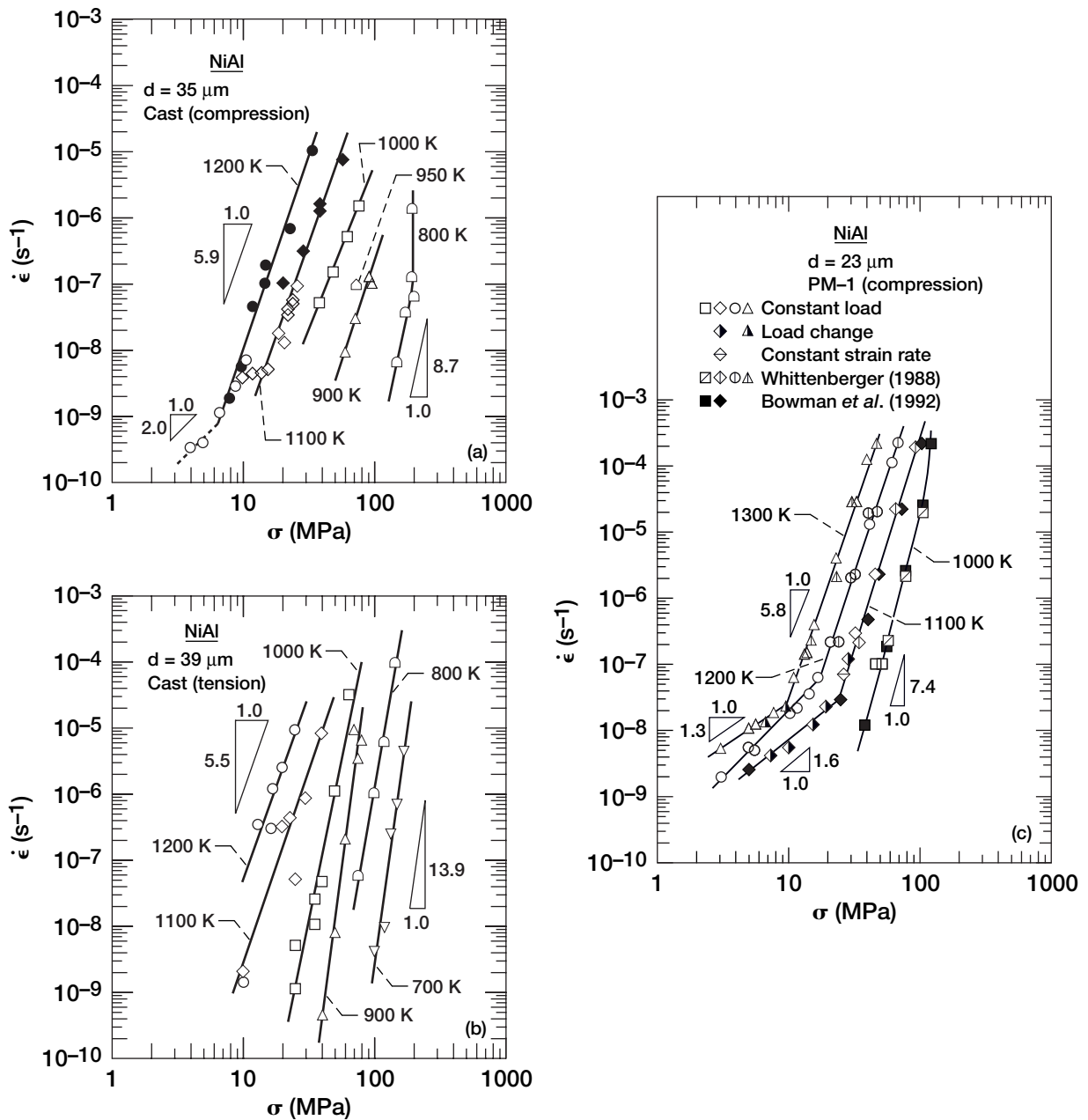


Figure 2.—Stress dependency of the true secondary creep rate for polycrystalline near-stoichiometric NiAl: (a) compression creep data for cast and extruded NiAl (ref. 15); (b) tension creep data for cast and extruded NiAl; and (c) compression creep data for PM-extruded NiAl (refs. 11 and 13). The closed and open symbols in (a) represent uninterrupted and interrupted tests, respectively. The literature data shown in (c) are from references 3 and 22.

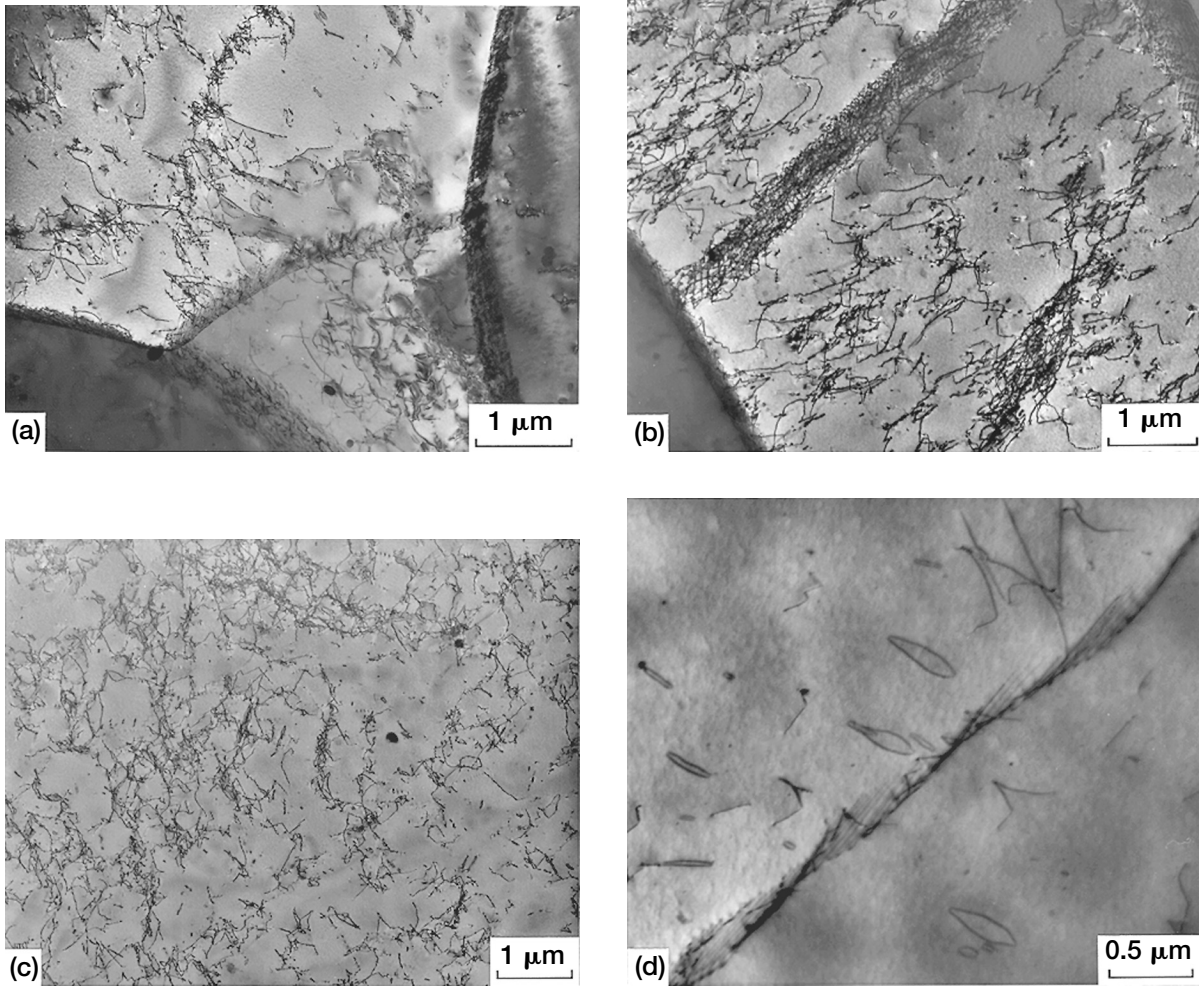


Figure 3.—Transmission electron micrographs of compression crept, near-stoichiometric, PM-extruded, polycrystalline NiAl showing (a) subgrains, (b) and (c) dislocation tangles and networks, (d) dipoles and elongated loops: (a–c) $T = 1200\text{ K}$; $\sigma = 41.3\text{ MPa}$; $\epsilon = 17.3\text{ pct.}$ (d) $T = 1200\text{ K}$; $\sigma = 29.2\text{ MPa}$; $\epsilon = 19.9\text{ pct.}$ (ref. 13).

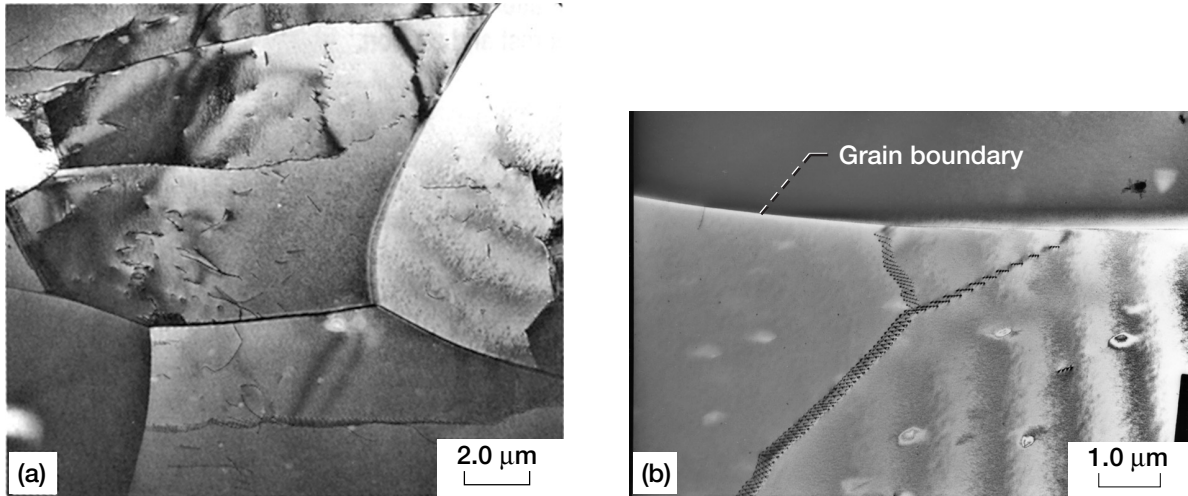


Figure 4.—Transmission electron micrographs of compression crept, near stoichiometric, cast and extruded, polycrystalline NiAl showing (a) well-formed subgrains and (b) grains showing little dislocation substructure: (a) $T = 1200\text{ K}$; $\sigma = 35\text{ MPa}$; $\epsilon = 15.5\text{ pct.}$ (ref. 15) (b) $T = 1200\text{ K}$; $\sigma = 25\text{ MPa}$; $\epsilon = 14.8\text{ pct.}$ (ref. 26).

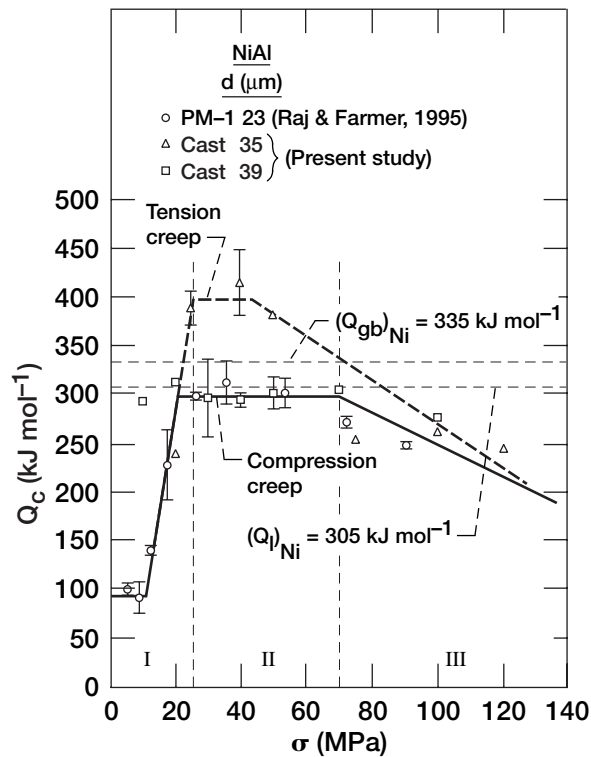


Figure 5.—Stress dependence of the true activation energy for creep for cast and PM-extruded polycrystalline, near-stoichiometric NiAl tested in compression and tension creep showing three deformation regimes. The values of $(Q_1)_{Ni}$ (ref. 28) and Q_c from the literature (refs. 11,13,14, and 16) are also included.

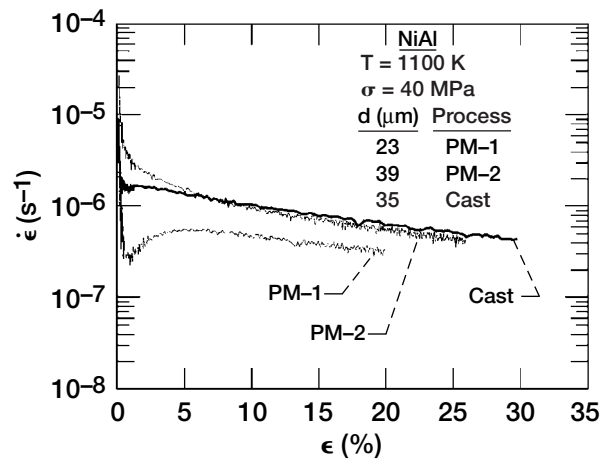


Figure 6.—True compressive creep rate versus true compressive strain for cast and PM-extruded polycrystalline NiAl demonstrating grain size strengthening in the finer-grained material (PM-1) (ref. 15).

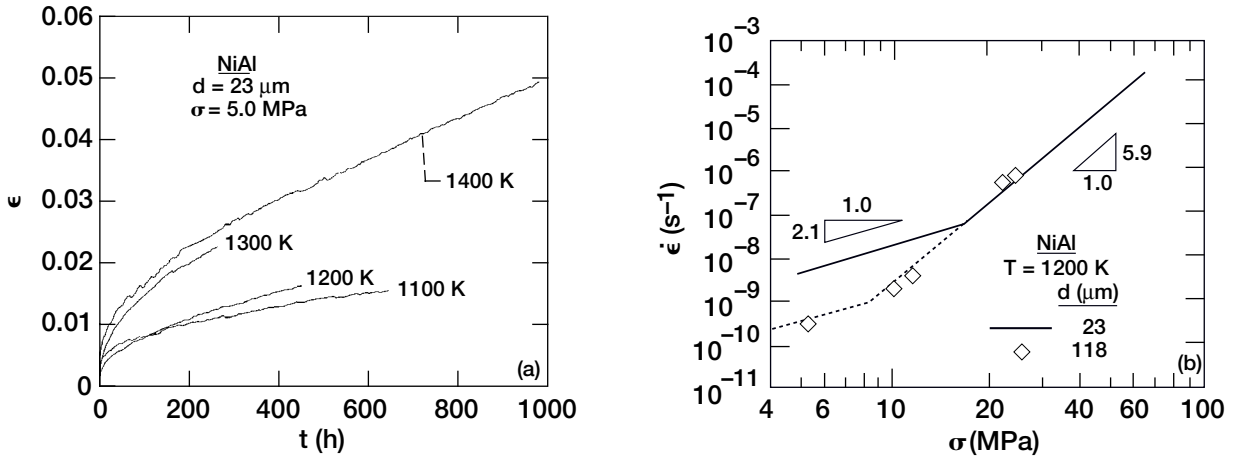


Figure 7.—(a) True compressive creep curves in region I showing a long normal primary creep behavior in NiAl; (b) Comparison of the stress dependence of the secondary creep rate at 1200 K for fine- and coarse-grained polycrystalline Ni-50.6Al in region I (ref. 13).

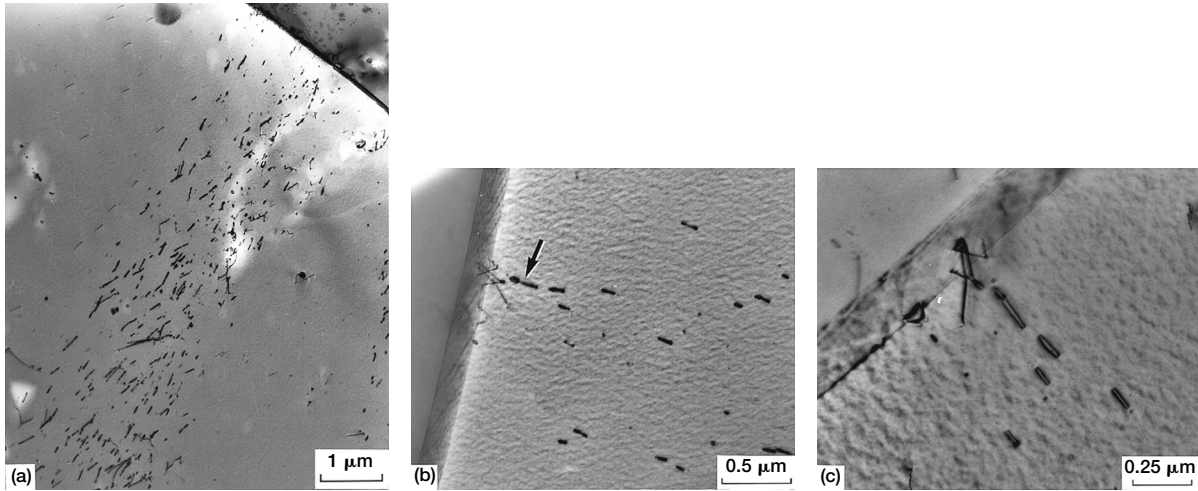


Figure 8.—Transmission electron micrographs showing the dislocation substructure formed in region I during creep of a polycrystalline, PM-extruded Ni-50.6Al alloy: (a) Bands of dislocation loops in a grain; $T = 1200\text{ K}$; $\sigma = 5.4\text{ MPa}$; $\epsilon = 3.1\text{ pct}$. (b) and (c) Emission of dislocation loops from the grain boundaries; $T = 1300\text{ K}$; $\sigma = 5.5\text{ MPa}$; $\epsilon = 2.3\text{ pct}$. The arrow in (b) shows the pinching of an elongated dislocation loop with the formation of a new loop (ref. 13).

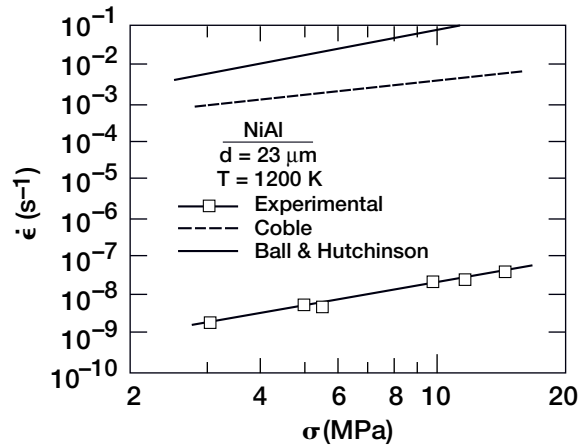


Figure 9.—Comparison of the experimental and predicted creep rates in region I.

REPORT DOCUMENTATION PAGE

Form Approved
OMB No. 0704-0188

Public reporting burden for this collection of information is estimated to average 1 hour per response, including the time for reviewing instructions, searching existing data sources, gathering and maintaining the data needed, and completing and reviewing the collection of information. Send comments regarding this burden estimate or any other aspect of this collection of information, including suggestions for reducing this burden, to Washington Headquarters Services, Directorate for Information Operations and Reports, 1215 Jefferson Davis Highway, Suite 1204, Arlington, VA 22202-4302, and to the Office of Management and Budget, Paperwork Reduction Project (0704-0188), Washington, DC 20503.

1. AGENCY USE ONLY (<i>Leave blank</i>)		2. REPORT DATE January 2002	3. REPORT TYPE AND DATES COVERED Technical Memorandum	
4. TITLE AND SUBTITLE Creep Behavior of Near-Stoichiometric Polycrystalline Binary NiAl			5. FUNDING NUMBERS WU-708-24-13-00	
6. AUTHOR(S) S.V. Raj				
7. PERFORMING ORGANIZATION NAME(S) AND ADDRESS(ES) National Aeronautics and Space Administration John H. Glenn Research Center at Lewis Field Cleveland, Ohio 44135-3191			8. PERFORMING ORGANIZATION REPORT NUMBER E-13015-1	
9. SPONSORING/MONITORING AGENCY NAME(S) AND ADDRESS(ES) National Aeronautics and Space Administration Washington, DC 20546-0001			10. SPONSORING/MONITORING AGENCY REPORT NUMBER NASA TM-2002-211210	
11. SUPPLEMENTARY NOTES Prepared for the 131st Annual Meeting and Exhibition sponsored by The Minerals, Metals, and Materials Society, Seattle, Washington, February 17-21, 2002. Portions of this material were presented at the meeting. Responsible person, S.V. Raj, organization code 5160, 216-433-8195.				
12a. DISTRIBUTION/AVAILABILITY STATEMENT Unclassified - Unlimited Subject Categories: 26, 24 and 07 Available electronically at http://gltrs.grc.nasa.gov/GLTRS This publication is available from the NASA Center for AeroSpace Information, 301-621-0390.			12b. DISTRIBUTION CODE	
13. ABSTRACT (<i>Maximum 200 words</i>) New and published constant load creep and constant engineering strain rate data on near-stoichiometric binary NiAl in the intermediate temperature range 700 to 1300 K are reviewed. Both normal and inverse primary creep curves are observed depending on stress and temperature. Other characteristics relating to creep of NiAl involving grain size, stress and temperature dependence are critically examined and discussed. At stresses below 25 MPa and temperatures above 1000 K, a new grain boundary sliding mechanism was observed with $n \sim 2$, $Q_c \sim 100 \text{ kJ mol}^{-1}$ and a grain size exponent of about 2. It is demonstrated that Coble creep and accommodated grain boundary sliding models fail to predict the experimental creep rates by several orders of magnitude.				
14. SUBJECT TERMS Creep; Intermetallic; NiAl; Activation energy; Dislocation microstructure; Creep mechanism			15. NUMBER OF PAGES 18	
			16. PRICE CODE	
17. SECURITY CLASSIFICATION OF REPORT Unclassified	18. SECURITY CLASSIFICATION OF THIS PAGE Unclassified	19. SECURITY CLASSIFICATION OF ABSTRACT Unclassified	20. LIMITATION OF ABSTRACT	